Mid-infrared supercontinuum generation in a suspended-core As_2S_3 chalcogenide microstructured optical fiber

Weiqing Gao,[1,*] Mohammed El Amraoui,[2] Meisong Liao,[1] Hiroyasu Kawashima,[1] Zhongchao Duan,[1] Dinghuan Deng,[1] Tonglei Cheng,[1] Takenobu Suzuki,[1] Younès Messaddeq,[2] and Yasutake Ohishi[1]

[1]*Research Center for Advanced Photon Technology, Toyota Technological Institute, 2-12-1, Hisakata, Tempaku, Nagoya 468-8511, Japan*
[2]*Centre d'optique, Photonique et Laser, Université Laval, Quebec, Pavillon Optique-Photonique, Canada*
[*]*weiqinggao@yahoo.com*

Abstract: We demonstrate the supercontinuum (SC) generation in a suspended-core As_2S_3 chalcogenide microstructured optical fiber (MOF). The variation of SC is investigated by changing the fiber length, pump peak power and pump wavelength. In the case of long fibers (20 and 40 cm), the SC ranges are discontinuous and stop at the wavelengths shorter than 3500 nm, due to the absorption of fiber. In the case of short fibers (1.3 and 2.4 cm), the SC ranges are continuous and can extend to the wavelengths longer than 4 μm. The SC broadening is observed when the pump peak power increases from 0.24 to 1.32 kW at 2500 nm. The SC range increases with the pump wavelength changing from 2200 to 2600 nm, corresponding to the dispersion of As_2S_3 MOF from the normal to anomalous region. The SC generation is simulated by the generalized nonlinear Schrödinger equation. The simulation includes the SC difference between 1.3 and 2.4 cm long fiber by 2500 nm pumping, the variation of SC with pump peak power in 2.4 cm long fiber, and the variation of SC with pump wavelength in 1.3 cm long fiber. The simulation agrees well with the experiment.

OCIS codes: (190.4370) Nonlinear optics, fibers; (320.6629) Supercontinuum generation; (060.5295) Photonic crystal fibers; (060.2390) Fiber optics, infrared.

References and links

1. T. M. Monro, W. Belardi, K. Furusawa, J. C. Baggett, N. G. R. Broderick, and D. J. Richardson, "Sensing with microstructured optical fibers," Meas. Sci. Technol. **12**(7), 854–858 (2001).
2. S. T. Cundiff and J. Ye, "Colloquium: Femtosecond optical frequency combs," Rev. Mod. Phys. **75**(1), 325–342 (2003).
3. I. Hartl, X. D. Li, C. Chudoba, R. K. Ghanta, T. H. Ko, J. G. Fujimoto, J. K. Ranka, and R. S. Windeler, "Ultrahigh-resolution optical coherence tomography using continuum generation in an air-silica microstructure optical fiber," Opt. Lett. **26**(9), 608–610 (2001).
4. D. L. Marks, A. L. Oldenburg, J. J. Reynolds, and S. A. Boppart, "Study of an ultrahigh-numerical-aperture fiber continuum generation source for optical coherence tomography," Opt. Lett. **27**(22), 2010–2012 (2002).
5. M. J. Thorpe, D. D. Hudson, K. D. Moll, J. Lasri, and J. Ye, "Cavity-ringdown molecular spectroscopy based on an optical frequency comb at 1.45-1.65 microm," Opt. Lett. **32**(3), 307–309 (2007).
6. J. M. Dudley, G. Genty, and S. Coen, "Supercontinuum generation in photonic crystal fiber," Rev. Mod. Phys. **78**(4), 1135–1184 (2006).
7. J. M. Dudley and J. R. Taylor, "Ten years of nonlinear optics in photonic crystal fibre," Nat. Photonics **3**(2), 85–90 (2009).
8. J. K. Ranka, R. S. Windeler, and A. J. Stentz, "Visible continuum generation in air-silica microstructure optical fibers with anomalous dispersion at 800 nm," Opt. Lett. **25**(1), 25–27 (2000).
9. J. C. Knight, T. A. Birks, P. St. J. Russell, and D. M. Atkin, "All-silica single-mode optical fiber with photonic crystal cladding," Opt. Lett. **21**(19), 1547–1549 (1996).
10. C. X. Yu, H. A. Haus, E. P. Ippen, W. S. Wong, and A. Sysoliatin, "Gigahertz-repetition-rate mode-locked fiber laser for continuum generation," Opt. Lett. **25**(19), 1418–1420 (2000).
11. W. Gao, M. Liao, L. Yang, X. Yan, T. Suzuki, and Y. Ohishi, "All-fiber broadband supercontinuum source with high efficiency in a step-index high nonlinear silica fiber," Appl. Opt. **51**(8), 1071–1075 (2012).

#183895 - $15.00 USD Received 22 Jan 2013; revised 6 Mar 2013; accepted 28 Mar 2013; published 10 Apr 2013

12. W. Gao, M. Liao, X. Yan, T. Suzuki, and Y. Ohishi, "All-fiber quasi-continuous wave supercontinuum generation in single-mode high-nonlinear fiber pumped by submicrosecond pulse with low peak power," Appl. Opt. **51**(13), 2346–2350 (2012).
13. J. S. Sanghera, L. B. Shaw, and I. D. Aggarwal, "Chalcogenide glass-fiber-based mid-IR sources and applications," IEEE J. Sel. Top. Quantum Electron. **15**(1), 114–119 (2009).
14. P. Petropoulos, H. Ebendorff-Heidepriem, V. Finazzi, R. C. Moore, K. Frampton, D. J. Richardson, and T. M. Monro, "Highly nonlinear and anomalously dispersive lead silicate glass holey fibers," Opt. Express **11**(26), 3568–3573 (2003).
15. H. Ebendorff-Heidepriem, P. Petropoulos, S. Asimakis, V. Finazzi, R. C. Moore, K. Frampton, F. Koizumi, D. J. Richardson, and T. M. Monro, "Bismuth glass holey fibers with high nonlinearity," Opt. Express **12**(21), 5082–5087 (2004).
16. G. Qin, X. Yan, C. Kito, M. Liao, C. Chaudhari, T. Suzuki, and Y. Ohishi, "Ultrabroadband supercontinuum generation from ultraviolet to 6.28 μm in a fluoride fiber," Appl. Phys. Lett. **95**(16), 161103 (2009).
17. M. Liao, W. Gao, Z. Duan, X. Yan, T. Suzuki, and Y. Ohishi, "Directly draw highly nonlinear tellurite microstructured fiber with diameter varying sharply in a short fiber length," Opt. Express **20**(2), 1141–1150 (2012).
18. M. Liao, W. Gao, Z. Duan, X. Yan, T. Suzuki, and Y. Ohishi, "Supercontinuum generation in short tellurite microstructured fibers pumped by a quasi-cw laser," Opt. Lett. **37**(11), 2127–2129 (2012).
19. P. Domachuk, N. A. Wolchover, M. Cronin-Golomb, A. Wang, A. K. George, C. M. B. Cordeiro, J. C. Knight, and F. G. Omenetto, "Over 4000 nm bandwidth of mid-IR supercontinuum generation in sub-centimeter segments of highly nonlinear tellurite PCFs," Opt. Express **16**(10), 7161–7168 (2008).
20. M. R. E. Lamont, B. Luther-Davies, D.-Y. Choi, S. Madden, and B. J. Eggleton, "Supercontinuum generation in dispersion engineered highly nonlinear (γ= 10 /W/m) As_2S_3 chalcogenide planar waveguide," Opt. Express **16**(19), 14938–14944 (2008).
21. X. Gai, D.-Y. Choi, S. Madden, Z. Yang, R. Wang, and B. Luther-Davies, "Supercontinuum generation in the mid-infrared from a dispersion-engineered As_2S_3 glass rib waveguide," Opt. Lett. **37**(18), 3870–3872 (2012).
22. N. D. Psaila, R. R. Thomson, H. T. Bookey, S. Shen, N. Chiodo, R. Osellame, G. Cerullo, A. Jha, and A. K. Kar, "Supercontinuum generation in an ultrafast laser inscribed chalcogenide glass waveguide," Opt. Express **15**(24), 15776–15781 (2007).
23. J. Troles, Q. Coulombier, G. Canat, M. Duhant, W. Renard, P. Toupin, L. Calvez, G. Renversez, F. Smektala, M. El Amraoui, J. L. Adam, T. Chartier, D. Mechin, and L. Brilland, "Low loss microstructured chalcogenide fibers for large non linear effects at 1995 nm," Opt. Express **18**(25), 26647–26654 (2010).
24. R. T. White and T. M. Monro, "Cascaded Raman shifting of high-peak-power nanosecond pulses in As_2S_3 and As_2Se_3 optical fibers," Opt. Lett. **36**(12), 2351–2353 (2011).
25. M. Duhant, W. Renard, G. Canat, T. N. Nguyen, F. Smektala, J. Troles, Q. Coulombier, P. Toupin, L. Brilland, P. Bourdon, and G. Renversez, "Fourth-order cascaded Raman shift in AsSe chalcogenide suspended-core fiber pumped at 2 μm," Opt. Lett. **36**(15), 2859–2861 (2011).
26. F. Smektala, C. Quemard, L. Leneindre, J. Lucasa, A. Barthélémy, and C. De Angelis, "Chalcogenide glasses with large non-linear refractive indices," J. Non-Cryst. Solids **239**(1-3), 139–142 (1998).
27. J. S. Sanghera, C. M. Florea, L. B. Shaw, P. Pureza, V. Q. Nguyen, M. Bashkansky, Z. Dutton, and I. D. Aggarwal, "Non-linear properties of chalcogenide glasses and fibers," J. Non-Cryst. Solids **354**(2-9), 462–467 (2008).
28. D.-I. Yeom, E. C. Mägi, M. R. E. Lamont, M. A. F. Roelens, L. Fu, and B. J. Eggleton, "Low-threshold supercontinuum generation in highly nonlinear chalcogenide nanowires," Opt. Lett. **33**(7), 660–662 (2008).
29. S. Dekker, C. Xiong, E. Magi, A. C. Judge, J. S. Sanghera, L. B. Shaw, I. D. Aggarwal, D. J. Moss, and B. J. Eggleton, "Broadband Low Power Super-continuum Generation in As_2S_3 Chalcogenide Glass Fiber Nanotapers," in *Conference on Lasers and Electro-Optic*s, Technical Digest (CD) (Optical Society of America, 2010), paper CMM6.
30. D. D. Hudson, S. A. Dekker, E. C. Mägi, A. C. Judge, S. D. Jackson, E. Li, J. S. Sanghera, L. B. Shaw, I. D. Aggarwal, and B. J. Eggleton, "Octave spanning supercontinuum in an As_2S_3 taper using ultralow pump pulse energy," Opt. Lett. **36**(7), 1122–1124 (2011).
31. W. Gao, M. Liao, X. Yan, C. Kito, T. Kohoutek, T. Suzuki, M. El-Amraoui, J.-C. Jules, G. Gadret, F. Désévédavy, F. Smektala, and Y. Ohishi, "Visible light generation and its influence on supercontinuum in chalcogenide As_2S_3 microstructured optical fiber," Appl. Phys. Express **4**(10), 102601 (2011).
32. M. El-Amraoui, G. Gadret, J. C. Jules, J. Fatome, C. Fortier, F. Désévédavy, I. Skripatchev, Y. Messaddeq, J. Troles, L. Brilland, W. Gao, T. Suzuki, Y. Ohishi, and F. Smektala, "Microstructured chalcogenide optical fibers from As_2S_3 glass: towards new IR broadband sources," Opt. Express **18**(25), 26655–26665 (2010).
33. M. El-Amraoui, J. Fatome, J. C. Jules, B. Kibler, G. Gadret, C. Fortier, F. Smektala, I. Skripatchev, C. F. Polacchini, Y. Messaddeq, J. Troles, L. Brilland, M. Szpulak, and G. Renversez, "Strong infrared spectral broadening in low-loss As-S chalcogenide suspended core microstructured optical fibers," Opt. Express **18**(5), 4547–4556 (2010).
34. Y. Yue, L. Zhang, Y. Yan, N. Ahmed, J.-Y. Yang, H. Huang, Y. Ren, S. Dolinar, M. Tur, and A. E. Willner, "Octave-spanning supercontinuum generation of vortices in an As_2S_3 ring photonic crystal fiber," Opt. Lett. **37**(11), 1889–1891 (2012).
35. S. Shabahang, M. P. Marquez, G. Tao, M. U. Piracha, D. Nguyen, P. J. Delfyett, and A. F. Abouraddy, "Octave-spanning infrared supercontinuum generation in robust chalcogenide nanotapers using picosecond pulses," Opt. Lett. **37**(22), 4639–4641 (2012).

#183895 - $15.00 USD Received 22 Jan 2013; revised 6 Mar 2013; accepted 28 Mar 2013; published 10 Apr 2013

36. I. Savelii, O. Mouawad, J. Fatome, B. Kibler, F. Désévédavy, G. Gadret, J.-C. Jules, P.-Y. Bony, H. Kawashima, W. Gao, T. Kohoutek, T. Suzuki, Y. Ohishi, and F. Smektala, "Mid-infrared 2000-nm bandwidth supercontinuum generation in suspended-core microstructured Sulfide and Tellurite optical fibers," Opt. Express **20**(24), 27083–27093 (2012).
37. A. Marandi, C. W. Rudy, V. G. Plotnichenko, E. M. Dianov, K. L. Vodopyanov, and R. L. Byer, "Mid-infrared supercontinuum generation in tapered chalcogenide fiber for producing octave-spanning frequency comb around 3 μm," Opt. Express **20**(22), 24218–24225 (2012).
38. R. R. Gattass, L. B. Shaw, V. Q. Nguyen, P. C. Pureza, I. D. Aggarwal, and J. S. Sanghera, "All-fiber chalcogenide-based mid-infrared supercontinuum source," Opt. Fiber Technol. **18**(5), 345–348 (2012).
39. J. Hu, C. R. Menyuk, L. B. Shaw, J. S. Sanghera, and I. D. Aggarwal, "Maximizing the bandwidth of supercontinuum generation in As_2Se_3 chalcogenide fibers," Opt. Express **18**(7), 6722–6739 (2010).
40. J. Hu, C. R. Menyuk, L. B. Shaw, J. S. Sanghera, and I. D. Aggarwal, "Computational study of 3-5 μm source created by using supercontinuum generation in As_2S_3 chalcogenide fibers with a pump at 2 μm," Opt. Lett. **35**(17), 2907–2909 (2010).
41. M. Bernier, M. El-Amraoui, J. F. Couillard, Y. Messaddeq, and R. Vallée, "Writing of Bragg gratings through the polymer jacket of low-loss As_2S_3 fibers using femtosecond pulses at 800 nm," Opt. Lett. **37**(18), 3900–3902 (2012).
42. G. P. Agrawal, *Nonlinear Fiber Optics 4th ed.* (Academic Press, 2007), Chap. 2.
43. T. Kohoutek, X. Yan, T. W. Shiosaka, S. N. Yannopoulos, A. Chrissanthopoulos, T. Suzuki, and Y. Ohishi, "Enhanced Raman gain of Ge-Ga-Sb-S chalcogenide glass for highly nonlinear microstructured optical fibers," J. Opt. Soc. Am. B **28**(9), 2284–2290 (2011).
44. C. Xiong, E. Magi, F. Luan, S. Dekker, J. S. Sanghera, L. B. Shaw, I. D. Aggarwal, and B. J. Eggleton, "Raman response in chalcogenide As_2S_3 fiber," in *14th OptoElectronics and Communications Conference*, Sydney, Australia, 13–17 July 2009, paper TuA2.

1. Introduction

In the past decades, supercontinuum (SC) generation in optical fibers has attracted extensive attention owing to its applications in fiber sensing [1], frequency metrology [2], optical coherence tomography [3, 4] and spectroscopy [5]. Supercontinua have the excellent properties such as wide spectral bandwidth, high coherence, high brightness and potential compactness [6–8]. Microstructured optical fibers (MOFs) or holey fibers have been successfully used for SC generation since they were first proposed by Knight et al. in early 90's [9]. MOFs have innovative properties such as high effective nonlinearity and tailorable dispersion profile [6, 7], as compared to traditional standard fibers.

Supercontinua generated in silica fibers have been demonstrated [8, 10–12]. However, the SC range stopped at the wavelengths shorter than 3 μm, due to the limit of the intrinsic transmission window of fused silica. Recent trend of SC research is to extend the spectral range to the mid-infrared (MIR) region (3-20 μm) for pushing the application further in military, medical, biologic and sensing systems [13]. Alternative materials to fused silica are necessary for generating the SCs at longer wavelengths in the MIR region. The alternative materials should possess the properties of large transmission window and high nonlinearity, simultaneously. Supercontinua generated in the fibers based on lead silicate [14], bismuth oxide [15], fluoride [16], tellurite [17–19] and chalcogenide glass [20–22] have been demonstrated. Qin et al. obtained the extremely wide SC from ultraviolet to 6.28 μm in a fluoride fiber by 50 MW pump peak power [16]. Domachuk et al. demonstrated over 4000 nm bandwidth of MIR SC generation in an 8 mm long tellurite photonic crystal fiber (PCF) [19].

Chalcogenide glass has great advantages due to their wider transmission window and higher nonlinearity in MIR region [23–27], as compared to the other materials mentioned above. Depending on the compositions, the chalcogenide glass can be transparent from the visible up to the infrared region of 12 or 15 μm; the nonlinear refractive index can be one- or several-order higher than silica, fluoride or tellurite glass. Many works about the SC generation in As-Se or As-S fibers have been demonstrated [28–38]. Yeom et al. [28] and Dekker et al. [29] demonstrated the SCs pumped by very low peak powers in As_2Se_3 and As_2S_3 tapered nanowires, respectively. Shabahang et al. [35] obtained octave-spanning SC in robust chalcogenide nanotapers using picosecond pulses. Savelii et al. [36] reported the SC generation from 1 to 3.2 μm in As_2S_3 chalcogenide fibers. Hu et al. computationally studied the SC generation in As_2Se_3 [39] and As_2S_3 PCF [40] to extend the range up to wavelengths

#183895 - $15.00 USD Received 22 Jan 2013; revised 6 Mar 2013; accepted 28 Mar 2013; published 10 Apr 2013

longer than 4 μm. It was possible to generate spectral range of SC longer than 4 μm by carefully selecting the waveguide parameters of the MOF as well as the peak power and duration of the pump pulse, according to the results by Hu et al. [39, 40]. Marandi et al. experimentally demonstrated the SC in the MIR region from 2.2 to 5 μm in a tapered As_2S_3 fiber [37], which was pumped by the pulses shorter than 100 fs centered around 3.1 μm from the subharmonic of a mode-locked Er-doped fiber laser. Gattass et al. [38] obtained the SC covering the wavelength range from 1.9 to 4.8 μm based on a combination of silica commercial components and an As_2S_3 step index optical fiber.

In this paper, we present the SC generation in a suspended-core As_2S_3 chalcogenide MOF. The variation of SC was investigated by changing the fiber length, pump peak power and pump wavelength. In the case of long fibers (20 and 40 cm), the SC ranges were discontinuous and stopped at the wavelengths shorter than 3500 nm, due to the absorption induced by the OH, SH and CO_2 contamination in the glass. In the case of short fibers (1.3 and 2.4 cm), the SC ranges were continuous and could extend to the wavelengths longer than 4 μm. The shift of soliton peak to longer wavelengths with the peak power increasing was observed. The SC range changed from narrow to wider when the pump wavelength was changed from 2200 to 2600 nm, corresponding to the dispersion of the As_2S_3 MOF from the normal to anomalous region. The SC generation was simulated by the generalized nonlinear Schrödinger equation. The simulation demonstrated that the SC evolution in theory was similar to that in experiment.

2. As_2S_3 chalcogenide MOF and experimental setup

The As_2S_3 chalcogenide MOF used in the experiment had a suspended-core structure with three holes, as shown in Fig. 1(a), measured by an optical microscope. The core diameter was ~3.2 μm, which was defined as the diameter of the circle inscribed in the triangular core. The sizes of holes were ~30-50 μm; the diameter of outer cladding was ~160 μm. The simulated fundamental mode-field profile at 2500 nm is shown in the inset of Fig. 1(b); the effective mode area was ~8.43 μm^2. The nonlinear coefficient at 2500 nm was calculated to be ~894.2 $W^{-1}km^{-1}$ according to the mode-field profile in the inset of Fig. 1(b) and the n_2 of 3×10^{-18} m^2W^{-1} in [33]. The attenuation was ~1 dB/m at 2000 nm measured by the cut-back technique. Figure 1(b) shows the chromatic dispersion profile simulated by commercial software (Lumerical Mode Solutions). The zero-dispersion wavelength (ZDW) was ~2.52 μm.

Figure 2 shows the experimental setup for the SC generation in the As_2S_3 MOF. The pump pulses used in the experiment were generated by an optical parametric oscillator (OPO) pumped by a Ti: sapphire laser with the wavelength of 800 nm. The wavelength of the OPO could be tuned from 1.7 to 3.2 μm; the repetition rate was 76 MHz; the full width at half maximum (FWHM) was ~200 fs. The output of the OPO was coupled into the As_2S_3 MOF by a Zinc Selenide (ZnSe) focusing lens with the focus length of 6 mm and numerical aperture (NA) of 0.25 at 3.75 μm. The ZnSe lens could transmit the wavelengths from 2 to 5 μm with the efficiency higher than 70%. The lengths of the As_2S_3 MOF used for measurement were from 1.3 to 40 cm. For each length, both fiber ends were cleaved well by a diamond stylus to ensure good cross sections. The As_2S_3 MOF was fixed on a precision stage with five dimensional adjustments. The coupling efficiency between the ZnSe lens and the As_2S_3 MOF was measured to be ~10%. The output end of the As_2S_3 MOF was butt connected to a 0.5 m large-mode-area (LMA) ZBLAN fiber with the core diameter of 105 μm and the transmission window from 0.4 to 5 μm. The output end of the ZBLAN fiber was connected directly to an optical spectrum analyzer (OSA) by a FC/PC connector, or was collimated to a FT-IR (Fourier-transform infrared) spectroscopy by a calcium fluoride (CaF_2) lens with the transmission window from 0.2 to 8 μm. The spectra in the range from 1200 to 2400 nm were measured by the OSA; the spectra longer than 2400 nm were measured by the FT-IR spectroscopy. Then the two spectral segments were spliced together.

#183895 - $15.00 USD Received 22 Jan 2013; revised 6 Mar 2013; accepted 28 Mar 2013; published 10 Apr 2013

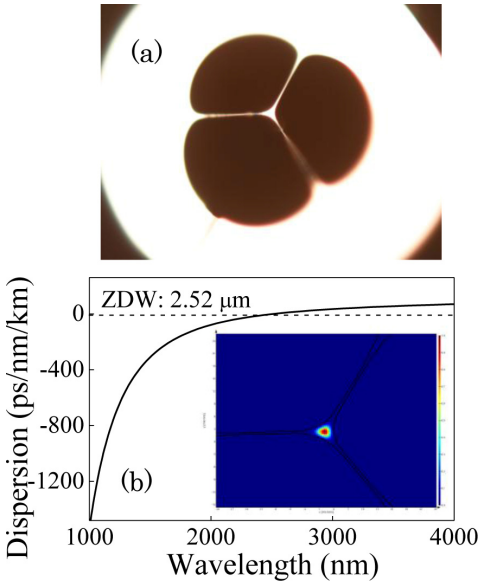

Fig. 1. (a) Cross section of the As_2S_3 chalcogenide MOF measured by an optical microscope. (b) Simulated chromatic dispersion of the As_2S_3 MOF. Inset: simulated fundamental mode-field profile at 2500 nm.

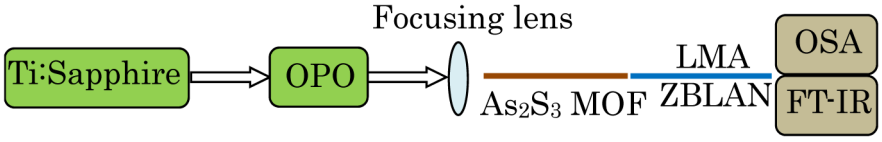

Fig. 2. Experimental setup for SC generation in the As_2S_3 MOF.

3. Experimental SC generation in the As_2S_3 MOF

3.1 SC generation in the fiber with different lengths

The repetition rate and FWHM of the pulse were maintained at 76 MHz and around 200 fs, respectively, when the wavelength of OPO was tuned from 1.7 to 3.2 μm. First, we used the pump pulse at 2500 nm close to the ZDW. The average power measured after the ZnSe lens was 201 mW. The peak power launched into the fiber was calculated to be 1.32 kW, considering the coupling efficiency. Figures 3(a)-3(e) show the SC generated in the As_2S_3 MOF with different lengths from 1.3 to 40 cm under the same pump condition. The SC range was considered according to the noise level.

In the case of long fibers [Figs. 3(a) and 3(b)], the SC ranges were discontinuous due to the absorption induced by the OH and SH contamination in the glass. When the fiber length was 40 cm [Fig. 3(a)], the SC range was from 1520 to 3360 nm with an absent region from 2610 to 3080 nm; the spectrum from 3080 to 3360 nm was weak. Decreasing the fiber length to 20 cm [Fig. 3(b)], the SC range was from 1540 to 3460 nm; the absent region was from 2720 to 2990 nm; the spectrum from 2990 to 3460 nm was strengthened. Decreasing the fiber length further to 10 cm [Fig. 3(c)], the SC range was from 1549 to 3795 nm; the absent region was from 2792 to 2890 nm; the absent range was decreased and the SC range was increased.

According to the results in Figs. 3(a)-3(c), the SC range was improved when the fiber absorption was reduced by shortening the length. Then we made the fiber shorter. In the case of short fibers [Figs. 3(d) and 3(e)], the absent regions in Figs. 3(a)-3(c) did not appear; the SC range of 2940 nm (from 1500 to 4440 nm) and 3020 nm (from 1510 to 4530 nm) were obtained in 1.3 and 2.4 cm fiber, respectively. The –20 dB bandwidth of SC in 1.3 and 2.4 cm

#183895 - $15.00 USD Received 22 Jan 2013; revised 6 Mar 2013; accepted 28 Mar 2013; published 10 Apr 2013

long fiber were 1258 nm (from 1752 to 3010 nm) and 1601 nm (from 1585 to 3186 nm), respectively. The difference of the absorption between 1.3 and 2.4 cm long fiber was not great, while the 2.4 cm long fiber provided higher nonlinear effects than 1.3 cm long fiber, such as the self-phase modulation (SPM) and soliton self-frequency shift (SSFS). The shift of soliton peak to longer wavelengths from Fig. 3(e) (dashed arrow) to Fig. 3(d) (dashed arrow) was observed when the fiber length was increased from 1.3 to 2.4 cm. This demonstrated that the effective nonlinear effects in 2.4 cm long fiber were stronger than those in 1.3 cm long fiber. Therefore, the SC generated in 2.4 cm long fiber had wider −20 dB bandwidth than that in 1.3 cm long fiber, while the whole SC range was similar. The spectra nearby 4 μm in Figs. 3(d) and 3(e) were weak due to the absorption induced by the SH and CO_2 contamination in the glass.

The material of the As_2S_3 MOF used in this work was the same as the single mode chalcogenide fiber used in [41]. According to Fig. 2 in [41], there was an obvious absorption due to OH contamination at around 2900 nm; the attenuation began to increase sharply at around 4 μm. The MID absorption at around 2900 nm corresponds to the absent region in Figs. 3(a)-3(c). The absent region shrank from Fig. 3(a) to Fig. 3(c) when the fiber length was decreased. The increase of attenuation at 4 μm of Fig. 2 in [41] corresponds to the reduced spectral intensity around 4 μm in Figs. 3(d) and 3(e).

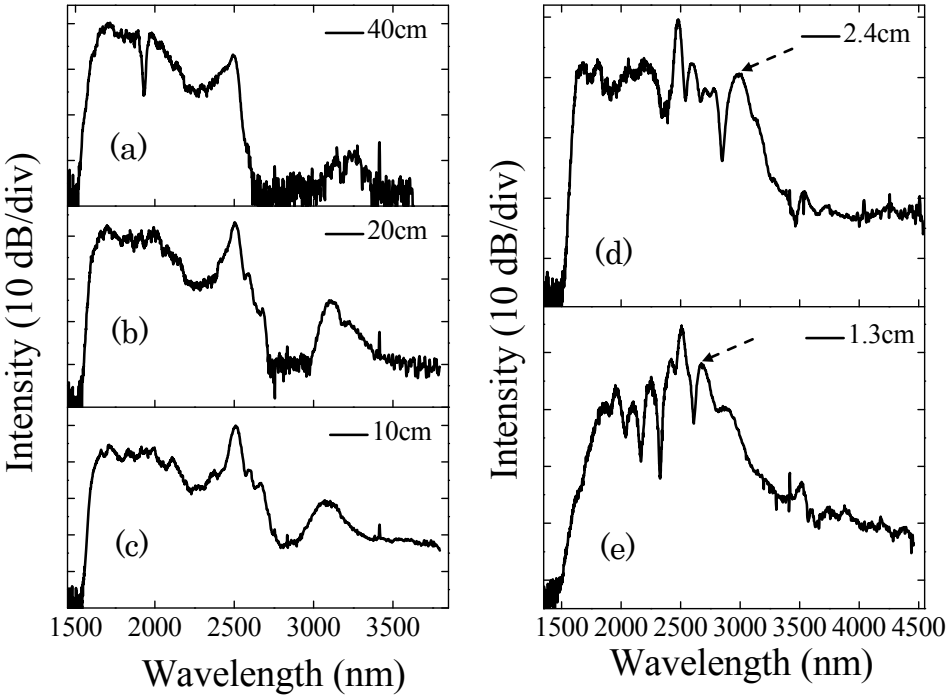

Fig. 3. Measured SCs in the As_2S_3 MOF with the fiber length of (a) 40, (b) 20, (c) 10, (d) 2.4, and (e) 1.3 cm at the pump wavelength of 2500 nm and pump peak power of 1.32 kW.

3.2 SC generation by different pump peak powers

The SC evolution with the pump peak power increasing from 0.24 to 1.32 kW at 2500 nm is shown in Figs. 4(a)-4(d), where the fiber length was 2.4 cm. With the peak power increasing from 0.24 to 1.32 kW, the nonlinear length $L_{NL} = 1/\gamma P_0$ decreased from 0.47 to 0.08 cm, where γ is the nonlinear coefficient and P_0 is the peak power. The dispersion length is $L_D = T_0^2/|\beta_2| \approx 3.1$ m, where $T_0 \approx T_{FWHM}/1.763$ is the pulse width for hyperbolic-secant shape and

#183895 - $15.00 USD Received 22 Jan 2013; revised 6 Mar 2013; accepted 28 Mar 2013; published 10 Apr 2013

β_2≈4.18 ps^2/km is the GVD parameter at 2500 nm calculated according to Fig. 1(b). The nonlinear effects were dominant in the 2.4 cm long fiber even with the low peak power as 0.24 kW because L_D was much larger than L_{NL}.

The SC generation was initiated by the SPM effect at the pump peak power of 0.24 kW, as shown in Fig. 4(a). The Raman solitons were formed, when the pump peak power was increased from 0.24 to 0.55 kW. The spectrum was broadened by the combined action of SPM, soliton, Raman and four-wave mixing (FWM) effect. When the peak power was increased further to 0.88 kW, the SC was broadened and the range of 2840 nm (from 1510 to 4350 nm) was obtained, as shown in Fig. 4(c). The SC range of 3020 nm (from 1510 to 4530 nm) was obtained at the maximum peak power of 1.32 kW, as shown in Fig. 4(d). The shift of soliton peak to longer wavelengths in Figs. 4(b)-4(d) (dashed arrows) was observed when the peak power was increased from 0.55 to 1.32 kW. In Fig. 4(d), the soliton number and soliton fission length were estimated to be about 62 and 5 cm [6], respectively. The estimation might be not accurate because the pulse width and peak power at the pump wavelength were used, which were a little different from those at soliton position.

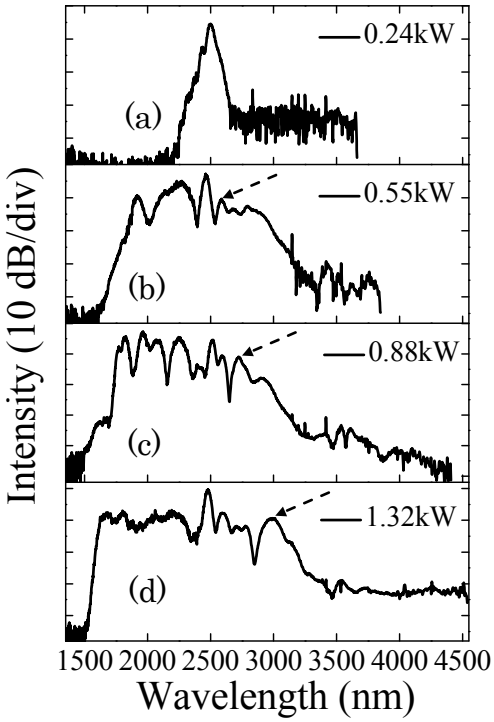

Fig. 4. Measured SCs in 2.4 cm long As_2S_3 MOF with the pump peak power increasing from 0.24 to 1.32 kW at the pump wavelength of 2500 nm.

3.3 SC generation by different pump wavelengths

The variation of SC was investigated when the wavelength of the OPO was adjusted from 2200 to 2600 nm, corresponding to the dispersion from the normal to anomalous region in Fig. 1(b). Figures 5(a)-5(h) show the SCs in 1.3 and 2.4 cm long As_2S_3 MOF at the pump wavelength of 2200, 2400, 2500 and 2600 nm, respectively. Due to the gain dispersion of the OPO, the average power measured after the focusing lens decreased from 265 to 192 mW for the wavelength from 2200 to 2600 nm, and the peak power launched into the fiber decreased from 1.74 to 1.26 kW as labeled in Figs. 5(a)-5(h).

#183895 - $15.00 USD Received 22 Jan 2013; revised 6 Mar 2013; accepted 28 Mar 2013; published 10 Apr 2013

Figure 5(a) shows the SC pumped by the wavelength of 2200 nm in the normal dispersion region far from the ZDW. The SC range was as narrow as 920 nm (from 1850 to 2770 nm), although the peak power of 1.74 kW was higher than other cases. The SC generation was dominated by the SPM effect in Fig. 5(a). The SC range increased to 1720 nm (from 1730 to 3450 nm) when the pump wavelength was changed to 2400 nm, as shown in Fig. 5(b). The SC in Fig. 5(b) was wider than that in Fig. 5(a) even the lower peak power of 1.34 kW was used. Figure 5(c) show the SC generated by the wavelength of 2500 nm near the ZDW; the range of 2940 nm (from 1500 to 4440 nm) was wider than that in Fig. 5(b) with the peak power of 1.32 kW. The wide SC of 3090 nm (from 1520 to 4610 nm) was obtained with the peak power of 1.26 kW, as shown in Fig. 5(d), when the pump wavelength was shifted further to 2600 nm in the anomalous dispersion region. The shift of soliton peak to longer wavelengths in Figs. 5(b)-5(d) (dashed arrows) was observed when the pump wavelength was changed from 2400 to 2600 nm. Figures 5(e)-5(h) show the variation of SC with the pump wavelengths corresponding to Figs. 5(a)-5(d). With the pump wavelength shifting from 2200 to 2600 nm, the variation of SC was similar to that in the 1.3 cm long fiber.

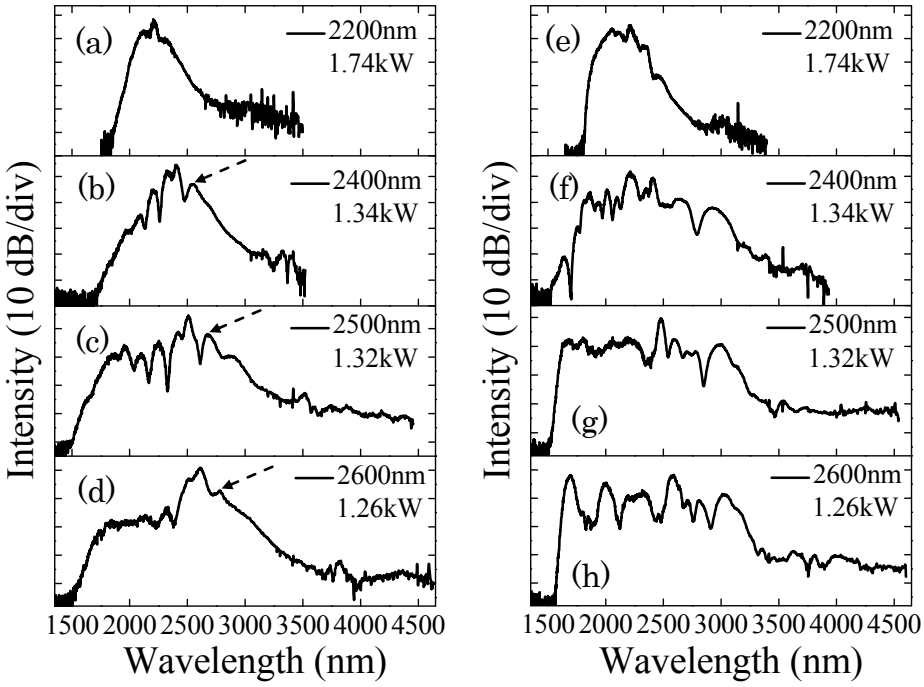

Fig. 5. Measured SCs in As_2S_3 MOF at different pump wavelengths from 2200 to 2600 nm. (a)-(d): 1.3 cm long fiber; (e)-(f): 2.4 cm long fiber.

4. Simulation for SC generation in the As_2S_3 MOF

The SC generation in the As_2S_3 MOF is modeled by the generalized nonlinear Schrödinger equation (GNLSE), expressed as [6, 42]

$$\frac{\partial A}{\partial z}+\frac{\alpha}{2}A-\sum_{k\geq 2}\frac{i^{k+1}}{k!}\beta_k\frac{\partial^k A}{\partial T^k}=i\gamma(1+\frac{i}{\omega_0}\frac{\partial}{\partial T})(A(z,T)\int_{-\infty}^{+\infty}R(T')\left|A(z,T-T')\right|^2dT'), \quad (1)$$

where $A(z,T)$ is the electric field envelope of the pump light in a retarded time frame $T = t-\beta_1 z$ moving at the group velocity $1/\beta_1$, β_k ($k\geq 2$) is the second and high-order dispersion terms, α is

#183895 - $15.00 USD Received 22 Jan 2013; revised 6 Mar 2013; accepted 28 Mar 2013; published 10 Apr 2013

the linear loss and ω_0 is the carrier frequency. The response function $R(t)$ includes both the instantaneous electronic, $\delta(t)$, and the delayed Raman contribution $h_R(t)$, expressed as

$$R(t) = (1-f_R)\delta(t) + f_R h_R(t), \tag{2}$$

$$h_R(t) = \frac{\tau_1^2 + \tau_2^2}{\tau_1 \tau_2^2} \exp(-t/\tau_2)\sin(t/\tau_1). \tag{3}$$

The f_R represents the fractional contribution of the delayed Raman response. The β_k ($k \geq 2$) can be calculated according to Fig. 1(b). The fiber length, pump peak power and pump wavelength are changed during the simulation. The other parameters used for the simulation are listed as in Table 1.

Table 1 Parameters Used for Simulation of the SC Generation in As_2S_3 MOF

Parameters	**Linear loss α**	**Nonlinear coefficient γ**	**Pulse width T_{FWHM}**	f_R [43]	τ_1 [44]	τ_2 [44]
Unit	dB/m	$W^{-1}km^{-1}$	fs	Null	fs	fs
Value	0	894.2@2500nm	200	0.031	15.2	230.5

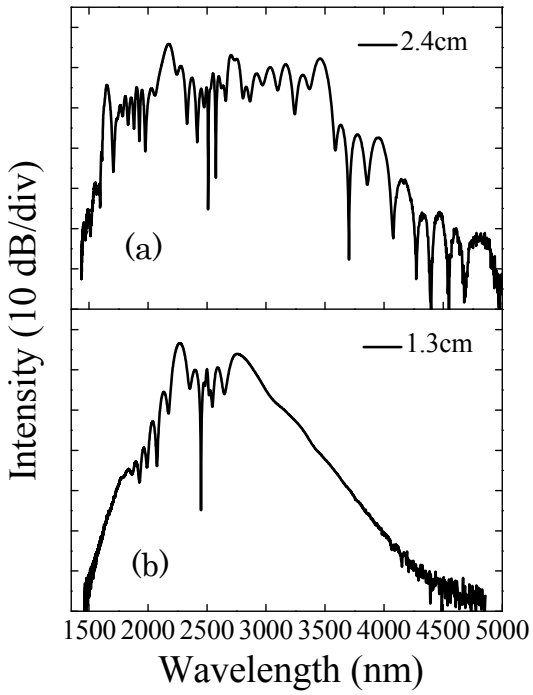

Fig. 6. Simulated SCs in the As_2S_3 MOF with the fiber lengths of 1.3 and 2.4 cm at the pump wavelength of 2500 nm and pump peak power of 1.32 kW.

Figures 6(a) and 6(b) show the simulated SCs in 2.4 and 1.3 cm long As_2S_3 MOF, respectively, where the pump peak power is 1.32 kW and the pump wavelength is 2500 nm. The SC ranges in Figs. 6(a) and 6(b) are 1450 to 4950 nm and 1490 to 4500 nm, respectively. The ranges are a little wider than those in Figs. 3(d) and 3(e). The spectral intensities in the range from 3000 to 4500 nm in Figs. 6(a) and 6(b) are stronger as compared to those in Figs. 3(d) and 3(e).

Figure 7(a) shows the simulated SCs in 2.4 cm long As_2S_3 MOF with the pump peak power increasing from 0.24 to 1.32 kW at the pump wavelength of 2500 nm. The SC is broadened with the peak power increasing. The soliton peak (dashed arrows) shifts to longer

#183895 - $15.00 USD Received 22 Jan 2013; revised 6 Mar 2013; accepted 28 Mar 2013; published 10 Apr 2013

wavelengths with the peak power increasing from 0.55 to 1.32 kW. The SC evolution in Fig. 7(a) is similar to that in Fig. 4. The soliton peaks of 0.55 and 0.88 kW pumping in Fig. 7(a) shift to longer wavelengths a little than those in Figs. 4(b) and 4(c). The simulated SC by 1.32 kW pumping in Fig. 7(a) shows more soliton peaks around 3000 nm than in Fig. 4(d).

Figure 7(b) shows the simulated SCs in 1.3 cm long As_2S_3 MOF with the pump wavelength changing from 2200 to 2600 nm. The nonlinear coefficient changed a little with the pump wavelength, which is calculated to be 1042.2, 939.5 and 852.4 $W^{-1}km^{-1}$ at 2200, 2400 and 2600 nm, respectively. The pump peak powers used in simulation are the same as those in Fig. 5. The SC is narrow when pumped at 2200 nm far from the ZDW. The SC is broadened by shifting the pump wavelength to 2400 nm. The spectral range extends to the region longer than 4 μm when pumped by the wavelengths of 2500 and 2600 nm. The soliton peaks shift to longer wavelengths (dashed arrows) for the pump wavelength from 2400 to 2600 nm. The SC evolution in Fig. 7(b) is similar to that in Figs. 5(a)-5(d), except that the positions of soliton peaks are a little longer shifting as compared to the experimental results.

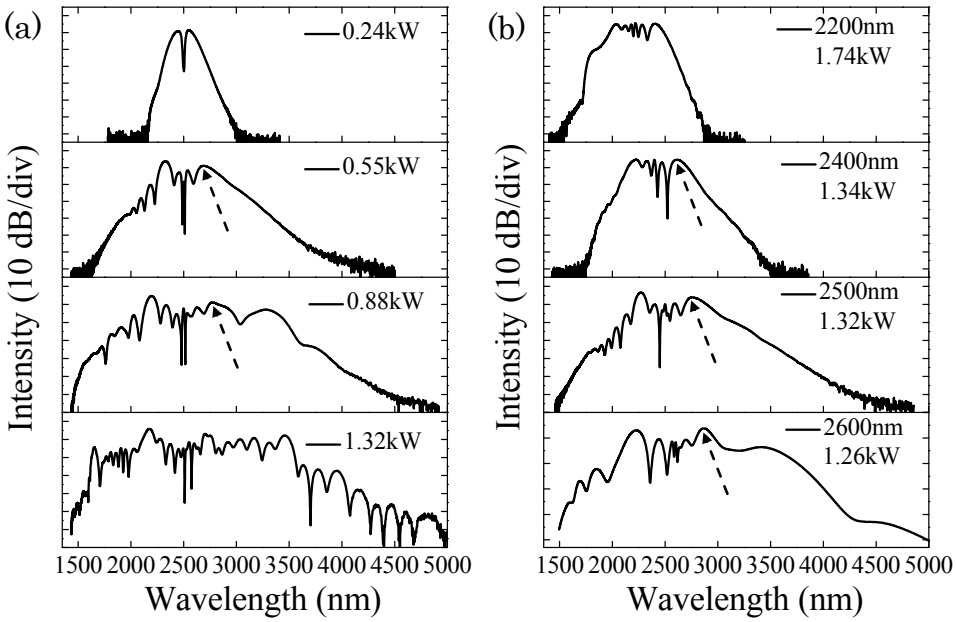

Fig. 7. (a) Simulated SCs in 2.4 cm long As_2S_3 MOF with different pump peak powers from 0.24 to 1.32 kW at the pump wavelength of 2500 nm. (b) Simulated SCs in 1.3 cm long As_2S_3 MOF at different pump wavelengths.

The results in Fig. 6 and Fig. 7 demonstrated that the SC evolution in the As_2S_3 MOF with the variation of fiber length, pump peak power and pump wavelength was similar between the simulation and experiment. The simulation could agree well with the experiment. There were still some differences between the simulation and experiment due to several reasons: (1) the absorption of the OH, SH and CO_2 contamination in the glass was not included in the theoretical model; (2) the deviation of the simulated dispersion profile in Fig. 1(b) would affect the shape and range of the simulated SC; (3) the transversal field profile of pump light was not considered; (4) the deviation of the measured coupling efficiency between the ZnSe lens and the As_2S_3 MOF would cause the difference of peak powers between the simulation and experiment. The simulation of the SC generation in the As_2S_3 MOF could agree with the experiment better, assuming that all the factors mentioned above would be considered in our future work.

The generated SC range in chalcogenide fiber is affected by several factors, such as dispersion profile, pump wavelength, pump peak power and fiber absorption et al. Compared

#183895 - $15.00 USD Received 22 Jan 2013; revised 6 Mar 2013; accepted 28 Mar 2013; published 10 Apr 2013

to other materials, chalcogenide fiber has higher nonlinearity and wider mid-infrared transmission range. In theory, it can generate the SC extending to the mid-infrared region, but no SC up to 8 μm in chalcogenide fiber has been reported so far. To achieve this goal, several possible ways should be considered. First, the higher peak power is necessary. In [16], Qin et al. obtained the SC to 6.28 μm using an extreme high peak power in fluoride fiber. Second, the longer pump wavelength up to 4 μm or longer region is suitable. In the simulation of [21], by shifting the pump wavelength from 3.26 to 3.68 μm, the SC was extended from 7 μm to longer wavelengths than 10 μm. Third, the absorptions caused by the OH, SH and CO_2 contamination in chalcogenide glass should be removed to guarantee that wide SC can transmit through the fiber.

5. Conclusion

We have demonstrated the SC generation in a suspended-core As_2S_3 chalcogenide MOF. The variation of SC was investigated by changing the experimental factors as fiber length, pump peak power and pump wavelength. The SCs extended to longer than 4 μm were obtained when the short fibers of 1.3 and 2.4 cm were used. The SC broadening was observed with the pump peak power increasing from 0.24 to 1.32 kW at 2500 nm. The SC range was relatively narrow when pumped by the wavelength in the normal dispersion far from the ZDW. With the pump wavelengths close to the ZDW, the SCs were wider and the soliton effect was observed. The SCs were simulated by the generalized nonlinear Schrödinger equation. The simulation demonstrated that the SC evolution in theory had the same ways as in experiment.

Acknowledgment

This work was supported by MEXT, Support Program for Forming Strategic Research Infrastructure (2011-2015).

#183895 - $15.00 USD Received 22 Jan 2013; revised 6 Mar 2013; accepted 28 Mar 2013; published 10 Apr 2013